AGU PUBLICATIONS

Paleoceanography

RESEARCH ARTICLE
10.1002/2015PA002795

# Southern Ocean control of glacial AMOC stability and Dansgaard-Oeschger interstadial duration

**Christo Buizert[1] and Andreas Schmittner[1]**

[1]College of Earth, Ocean and Atmospheric Sciences, Oregon State University, Corvallis, Oregon, USA

**Key Points:**
- DO interstadial duration is strongly correlated with Antarctic temperature
- Warming (cooling) the SO in model simulations strengthens (weakens) the AMOC
- We propose SH climate control on AMOC stability and DO timing

**Supporting Information:**
- Text S1, Data Set S1, and Audio S1
- Source Codes S1

**Correspondence to:**
C. Buizert,
buizertc@science.oregonstate.edu

**Citation:**
Buizert, C., and A. Schmittner (2015), Southern Ocean control of glacial AMOC stability and Dansgaard-Oeschger interstadial duration, *Paleoceanography*, *30*, 1595–1612, doi:10.1002/2015PA002795.

Received 24 FEB 2015
Accepted 15 OCT 2015
Accepted article online 21 OCT 2015
Published online 5 DEC 2015



**Abstract** Glacial periods exhibit abrupt Dansgaard-Oeschger (DO) climatic oscillations that are thought to be linked to instabilities in the Atlantic meridional overturning circulation (AMOC). Great uncertainty remains regarding the dynamics of the DO cycle, as well as controls on the timing and duration of individual events. Using ice core data we show that the duration of warm (interstadial) periods is strongly correlated with Antarctic climate, and presumably with Southern Ocean (SO) temperature and the position of the Southern Hemisphere (SH) westerlies. We propose a SO control on AMOC stability and interstadial duration via the rate of Antarctic bottom water formation, meridional density/pressure gradients, Agulhas Leakage, and SO adiabatic upwelling. This hypothesis is supported by climate model experiments that demonstrate SO warming leads to a stronger AMOC that is less susceptible to freshwater perturbations. In the AMOC stability diagram, SO warming and strengthening of the SH westerlies both shift the vigorous AMOC branch toward higher freshwater values, thus raising the threshold for AMOC collapse. The proposed mechanism could provide a consistent explanation for several diverse observations, including maximum DO activity during intermediate ice volume/SH temperature, and successively shorter DO durations within each Bond cycle. It may further have implications for the fate of the AMOC under future global warming.

## 1. Introduction

The Atlantic meridional overturning circulation (AMOC) plays a key role in the global climate system. It consists of a warm, northward flow in the near-surface Atlantic, the formation of North Atlantic Deep Water (NADW) in the Greenland and Labrador seas, and southward return flow at depth. Because the return flow is colder than the near-surface flow, the AMOC effectively transports heat from the Southern Hemisphere (SH) to the Northern Hemisphere (NH) [*Crowley*, 1992]. Perturbations to the AMOC strength are thus expected to impact climate of both hemispheres oppositely, a phenomenon commonly referred to as the thermal bipolar seesaw effect [*Mix et al.*, 1986; *Crowley*, 1992; *Broecker*, 1998; *Stocker and Johnsen*, 2003].

The most dramatic expression of AMOC instability is thought to have occurred during glacial times, where it has been associated with abrupt Dansgaard-Oeschger (DO) oscillations (Figure 1a) [*Dansgaard et al.*, 1982]. During DO warming events, central Greenland temperatures increase by as much as 8–15°C in several decades, with a warming pattern over Greenland that fingerprints a North Atlantic origin [*Guillevic et al.*, 2013; *Buizert et al.*, 2014]. While many studies suggest the involvement of AMOC variations in DO variability [e.g., *Oppo and Lehman*, 1995; *Curry and Oppo*, 1997; *Zahn et al.*, 1997; *Keigwin and Boyle*, 1999; *Clark et al.*, 2002; *Barker et al.*, 2009], great uncertainty remains regarding the dynamics and trigger of the DO events. Proposed mechanisms include sea ice variability [*Gildor and Tziperman*, 2003; *Li et al.*, 2005; *Dokken et al.*, 2013], freshwater forcing [*Manabe and Stouffer*, 1995; *Ganopolski and Rahmstorf*, 2001], ice shelf collapse [*Petersen et al.*, 2013], changing storm tracks [*Seager and Battisti*, 2007; *Wunsch*, 2006], $CO_2$ variations driven by Southern Ocean (SO) upwelling [*Banderas et al.*, 2012, 2014], and the tropical Pacific [*Clement et al.*, 2001]. The DO events may represent some of the largest and most abrupt reorganizations of oceanic transport during the Quaternary, and developing a complete understanding of their dynamics is a key goal of paleoclimate research.

Reorganization of the AMOC during the DO cycle probably consists of a number of closely linked changes that include, but are not limited to, variations in AMOC strength [*McManus et al.*, 2004], the mechanism and location of NADW (or rather GNAIW, Glacial North Atlantic Intermediate Water) formation [*Dokken and Jansen*, 1999; *Wang and Mysak*, 2006], deep water circulation and provenance [*Gutjahr et al.*, 2010; *Martrat et al.*, 2007;

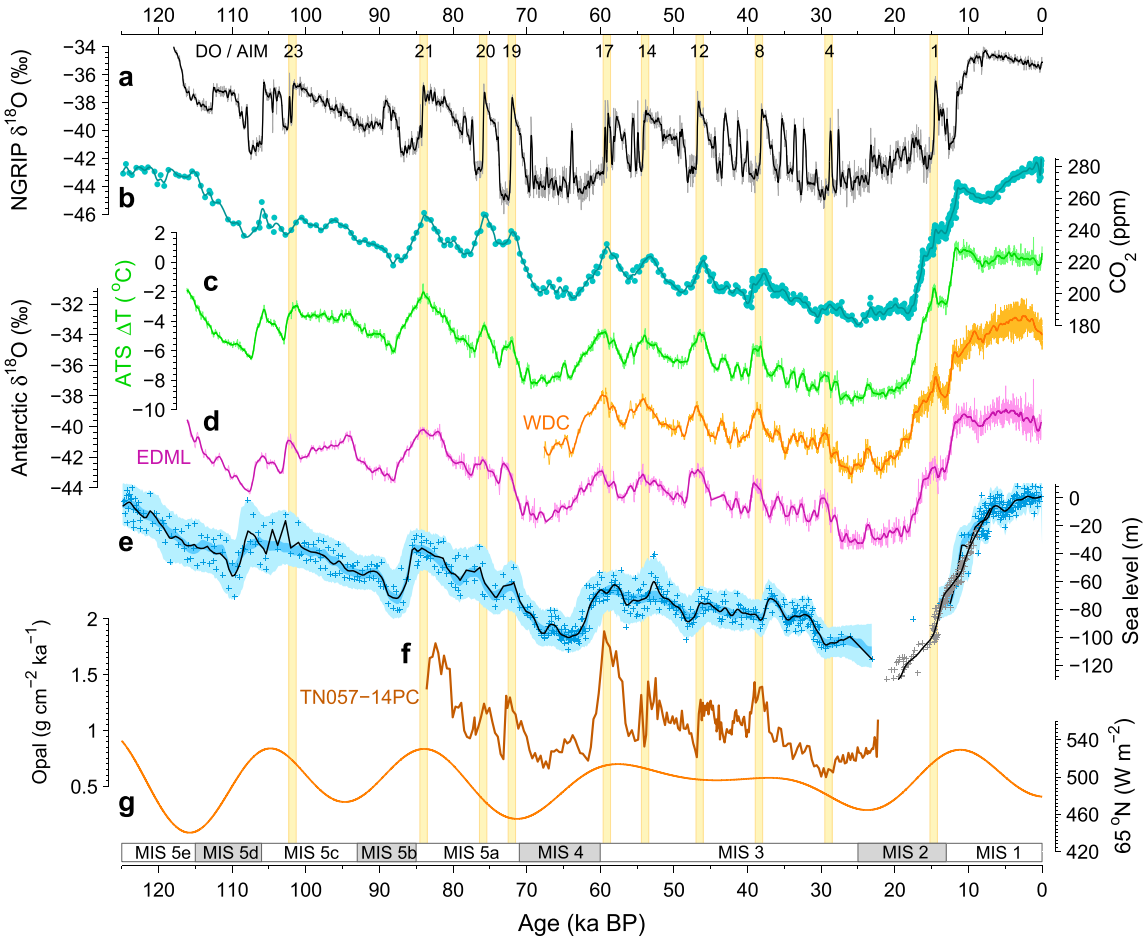


**Figure 1.** Climate records of the last glacial period. (a) Greenland ice core $\delta^{18}O$ from the North Greenland Ice Core Project (NGRIP) core [*NGRIP Community Members*, 2004] on the GICC05modelext chronology [*Rasmussen et al.*, 2006, 2013]. (b) Atmospheric $CO_2$ composite record [*Bereiter et al.*, 2015]. (c) Antarctic temperature stack (ATS, green) in °C relative to present day [*Parrenin et al.*, 2013]. (d) Antarctic ice core $\delta^{18}O$ from the EPICA Dronning Maud Land (EDML) (purple) and West Antarctic Ice Sheet (WAIS) Divide ice core (orange) [*EPICA Community Members*, 2006; *WAIS Divide Project Members*, 2015]. (e) Relative sea level. Blue crosses, solid curve, and shading give Red Sea sea level data the 1 ka smoothed record (Gaussian filter) and the $\pm 2\sigma$ uncertainty envelope, respectively [*Grant et al.*, 2012; *Rohling et al.*, 2009]. Grey crosses and solid curve give the compiled sea level data and reconstruction, respectively, by *Carlson and Clark* [2012]. (f) Southern Ocean opal flux as a proxy for upwelling from marine sediment core TNO57-14PC [*Anderson et al.*, 2009], using an updated chronology [*Obrochta et al.*, 2014]. (g) Milanković forcing: summer solstice insolation at 65°N. Yellow vertical bars with numbering denote the major DO/Antarctic isotopic maximum events.

*Piotrowski et al.*, 2008; *Vidal et al.*, 1997], and the extent of sea ice in the North Atlantic [*Li et al.*, 2005; *Broecker*, 2006]. Here we shall use "stadial AMOC mode" and "interstadial AMOC mode" as a shorthand to describe the states associated with a weak AMOC/cold North Atlantic and with a strong AMOC/warm North Atlantic, respectively. A third glacial AMOC mode has been associated with Heinrich events—periods of extreme cold in the North Atlantic, identified by layers of ice-rafted debris in ocean sediments [*Hemming*, 2004; *Rahmstorf*, 2002]. In this mode, the AMOC is thought to be at its weakest, with strongly reduced GNAIW formation and enhanced intrusion of southern-sourced waters into the North Atlantic [*Vidal et al.*, 1997; *Keigwin and Boyle*, 1999; *Martrat et al.*, 2007; *Böhm et al.*, 2015].

Not all DO cycles are created equal, as their duration, recurrence time and magnitude varies through time. Detecting structure within the DO time series is complicated by both chronological uncertainties and the limited number of event realizations in the Greenland ice core record (25 DO events have been identified in the last glacial). Some of the commonly recognized patterns include the following:

1. DO events, particularly those of marine isotope stage (MIS) 3, appear to be grouped into so-called Bond cycles [*Bond et al.*, 1993; *Lehman*, 1993] that are separated by Heinrich events; successive DO events within each Bond cycle have a decreasing interstadial duration and amplitude.

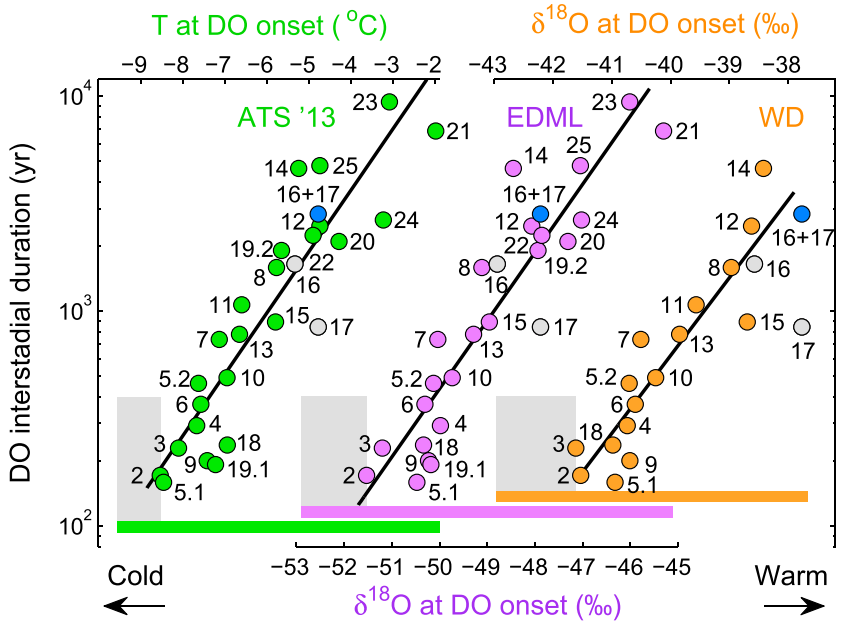


**Figure 2.** Correlation between Antarctic temperature and DO interstadial duration for the Antarctic Temperature Stack (ATS, green) [*Parrenin et al.*, 2013], the EPICA (European Project for Ice Coring in Antarctica) Dronning Maud Land core (EDML, purple) [*EPICA Community Members*, 2006], and the WAIS Divide core (WD, orange) [*WAIS Divide Project Members*, 2015], with DO events numbered. Colored bars near the figure bottom give the temperature/$\delta^{18}$O range spanned by the Antarctic records; the grey areas denote the coldest phase of the records during which DO events are absent. Black lines show a linear fit; the coefficient of determination is $R^2$ = 0.84, 0.87, and 0.86 for ATS, EDML, and WD, respectively. In this plot, Antarctic temperatures are evaluated at the onset of the corresponding NH interstadial period; similar results are obtained when evaluating the average Antarctic temperature over the duration of the interstadial. Interstadial durations are determined from $\delta^{18}$O of the NGRIP ice core [*NGRIP Community Members*, 2004]; see *Buizert et al.* [2015] for details.

2. DO variability is greatest at times of intermediate ice volume [*McManus et al.*, 1999; *Schulz et al.*, 1999; *Sima et al.*, 2004]; DO events are absent during MIS 2 and MIS 4 when global ice volume is large (Figure 1e), and also during interglacial periods when global ice volume is low.
3. Several studies have suggested that the events are spaced by 1470 years, or multiples thereof [*Grootes and Stuiver*, 1997; *Alley et al.*, 2001; *Schulz*, 2002], possibly reflecting an external (solar) forcing [e.g., *Braun et al.*, 2005]. This DO periodicity has been disputed, however, and is not present when using the most current Greenland ice core chronology (GICC05) [*Ditlevsen et al.*, 2005, 2007]. Instead, it has been suggested that the event recurrence time is consistent with simple stochastic models in which the events are purely noise induced [*Ditlevsen*, 1999; *Ditlevsen et al.*, 2005; *Braun et al.*, 2011].

Studies of DO dynamics have mostly focused on processes in the North Atlantic to modify the strength and stability of the AMOC. Recent work in physical oceanography suggests an important role of Southern Ocean (SO) processes in setting the rates of the global overturning circulation [e.g., *Toggweiler and Russell*, 2008; *Sijp and England*, 2009; *Beal et al.*, 2011; *Marshall and Speer*, 2012; *Talley*, 2013; *Ferrari*, 2014]. Investigating the role of SO processes on the DO cycle is therefore a natural line of inquiry. Here we propose that the stability of the AMOC and the timing characteristics of DO oscillations are linked to SH climate, via the influence of SO processes on the AMOC.

## 2. AMOC Stability and the Timing Characteristics of the DO Cycle

### 2.1. DO Interstadial and Stadial Durations

The key observation in this work is shown in Figure 2, where we plotted the Greenland interstadial duration (logarithmic scale) versus the $\delta^{18}$O (or temperature) of Antarctic ice cores. For each of the three Antarctic records evaluated (see figure caption for details), we observe a similar pattern: during periods when Antarctic temperatures are high, such as during MIS 5, DO interstadial periods tend to be long. By contrast, during Antarctic cold periods, such as MIS 2 and 4, DO interstadials tend to be short. During the coldest parts of the Last Glacial Maximum (LGM) (indicated as shaded grey areas in Figure 2), DO events are completely absent.

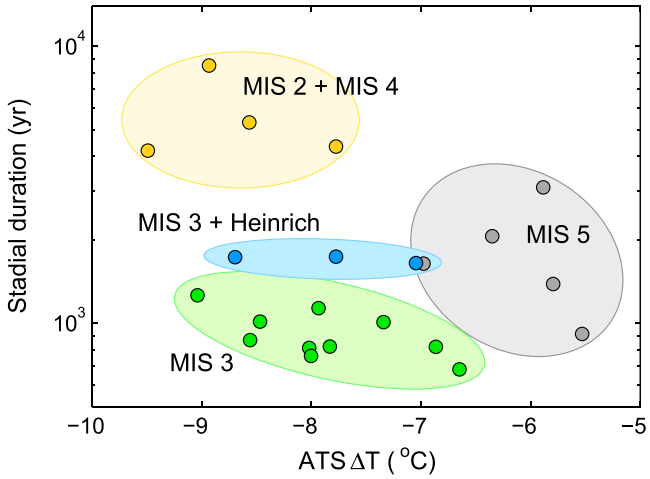


**Figure 3.** Correlation between Antarctic temperature and DO stadial duration. Stadial periods of MIS 2 and MIS 4 are marked in yellow (GS 2.1, 3, 18, and 19.1); MIS 3 Heinrich stadials are marked in blue (GS 5.1, 9, and 13), all other MIS 3 stadials are marked in green; MIS 5 stadials are marked in grey; stadials that are not fully developed in the record (<400 years) are omitted (GS 14, 17, and 23), as they do not represent full baseline separation of DO events.

We thus observe a strong correlation between Antarctic temperature and the logarithm of the duration of the concomitant NH interstadial period ($r$ of 0.92 to 0.94, depending on the Antarctic core used).

For all three Antarctic records investigated, DO 17 appears to fall besides the trend line, due to its relatively short interstadial duration. Both DO 16 and DO 17 are anomalous among the DO events, as they are composed of a series of short-duration pulses, separated by unusually short stadial periods. Their separation into two events is therefore somewhat arbitrary. If the durations of DO 16 and 17 are added together (blue dots), the combined event falls onto the trend line. Perhaps, DO 16 and 17 form a single interstadial period, repeatedly interrupted by meltwater pulses from the circum-North Atlantic ice sheets that are retreating from their MIS 4 highstand (Figure 1e).

The relationship between Greenland stadial duration and SH high-latitude temperature is not nearly as clear (Figure 3). Stadial durations of MIS 2 and 4 are the longest in the record, and they occur at times of Antarctic cold. All the stadial periods of MIS 3 have a comparable duration (marked in green), with the exception of the Heinrich stadials, which tend to be $\sim 10^3$ years longer (marked in blue). Stadial durations during MIS 5, when the SH was relatively warm, are on average slightly longer than those of MIS 3 and roughly comparable to those of the Heinrich stadials. The more complex pattern of Figure 3 may reflect a more varied number of controls on stadial duration. In particular, the influence of freshwater input into the North Atlantic is important, as is clear from the elongated duration of Heinrich stadials.

Antarctic ice cores provide reliable, well-dated, high-resolution records of SH high-latitude surface air temperature throughout the glacial period [*Jouzel et al.*, 1997, 2003]. Sea surface temperature (SST) records of comparable resolution and age control are unavailable from the SO itself, in large part due to the poor preservation of foraminifera in corrosive SO deep water, the cold environment that poses a calibration problem for the use of the alkenone unsaturation index, and stratigraphic disturbances caused by turbidites and sediment winnowing by the strong bottom currents of the Antarctic Circumpolar Current (ACC). We will here assume that Antarctic temperature is closely linked to SO SST and can be used as a measure thereof; this assumption is supported by available reconstructions from the SO [*Barrows et al.*, 2007; *Lopes Dos Santos et al.*, 2012].

### 2.2. The Hypothesis

We propose that the timing characteristics of the DO cycles are controlled by SH climate through the influence of SO processes on the strength and stability of the AMOC. During periods of SH (high-latitude) warmth, the vigorous interstadial AMOC mode is more stable. This stability allows the interstadial mode to persist longer periods of time, which is reflected by long interstadial durations. With cooling SH high-latitude temperatures, the interstadial AMOC mode becomes increasingly unstable, resulting in shorter interstadial durations.

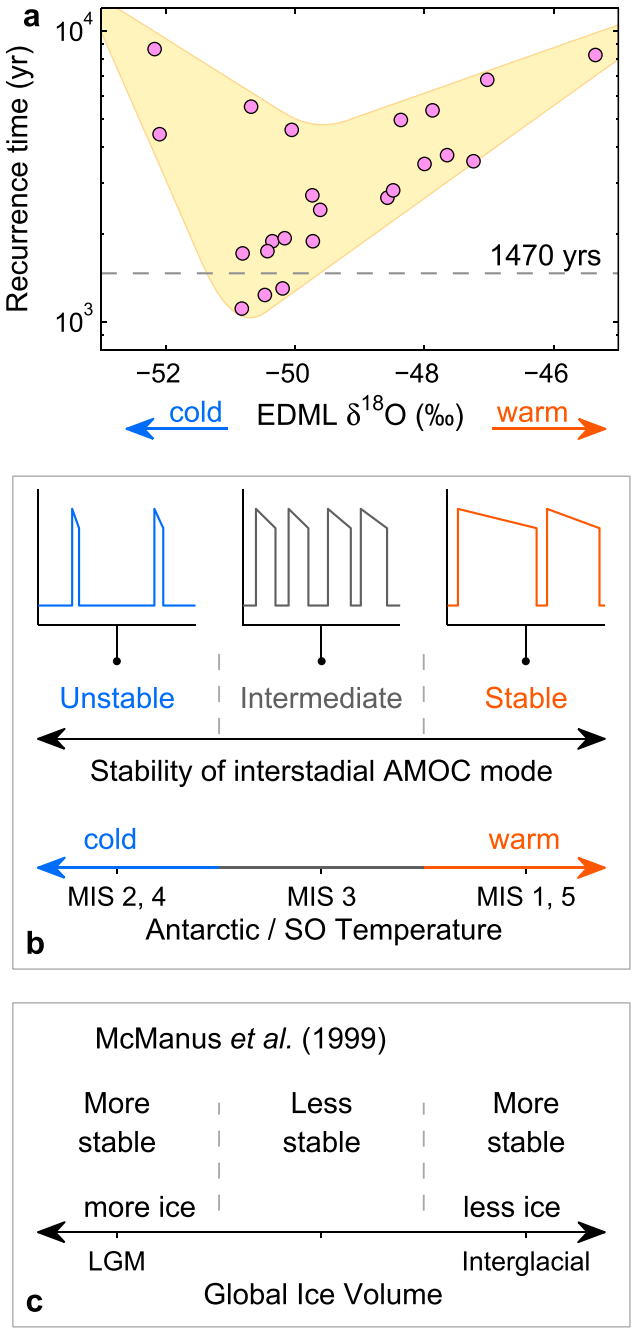


**Figure 4.** DO recurrence time and AMOC stability. (a) Recurrence time of DO events as a function of Antarctic temperature. (b) Schematic representation of our hypothesis of AMOC stability and DO timing. (c) Schematic representation of the ice-volume hypothesis redrawn from *McManus et al.* [1999].

During MIS 2, when SH high latitudes are at their coldest, DO events are absent as the interstadial AMOC mode has become too unstable to persist for any amount of time; the absence of DO events results in long stadial durations. Our hypothesis is depicted schematically in Figure 4b.

Our hypothesis does not favor any specific dynamical pathway for a DO event to unfold, nor do we mean to suggest (or dispute) that the SH high latitudes control the timing of any individual event (as suggested by *Knorr and Lohmann* [2003]). Rather, SH high-latitude climate sets the background condition of AMOC stability under which the DO cycle operates, and in doing so it controls the DO timing characteristics. Our hypothesis is therefore compatible with most of the proposed DO mechanisms and triggers.

Note that our hypothesis does not encompass the stability of the stadial AMOC mode. The long stadial durations of MIS 2 and MIS 4 may simply reflect the absence of DO events; if those events (marked in yellow in Figure 3) are not considered, there is no clear relationship between stadial duration and SH conditions.

### 2.3. DO Recurrence Times

The DO recurrence (or waiting) time equals the number of years between subsequent DO warming events, and as such each recurrence time is the sum of one stadial and one interstadial duration. In Figure 4a we have plotted DO recurrence times as a function of Antarctic temperature. Long DO recurrence times are observed both when the SH high latitudes are relatively warm (due to a lengthening of the interstadial durations as in Figure 2) and when the SH high latitudes are cold (due to long stadial durations in the absence of DO events, as in Figure 3). The shortest recurrence times are found during periods of intermediate SH high-latitude temperatures. This V-shaped pattern suggests a (deterministic) control on DO recurrence time, contrary to the suggestion that DO recurrence times are purely stochastic [*Ditlevsen et al.*, 2005; *Braun et al.*, 2011]. We likewise find no evidence that DO recurrence times cluster around multiples of 1470 years. There appears to be a threshold around an EDML $\delta^{18}$O value of −51 (Figure 4a); above this value, recurrence times change gradually as interstadial durations can take any value (and stadial durations are more or less constant); below this value, recurrence time increases instantly as DO events virtually disappear.

Short recurrence times are equivalent to high climatic variability, and as such we suggest that maximum DO variability occurs during periods of intermediate SO temperatures (as during MIS 3). Earlier studies have suggested a link between DO variability and global ice volume instead [*McManus et al.*, 1999; *Schulz et al.*, 1999; *Sima et al.*, 2004], and maximum climate variability during periods of intermediate ice volume. Due to the high correlation between SH high-latitude temperature and global ice volume (Figure 1), both statements are equivalent (periods of intermediate global ice volume are also periods of intermediate SH high-latitude temperature). The schematic stability diagram suggested by *McManus et al.* [1999] is reproduced in Figure 4c. It suggests the existence of a "Goldilocks" zone of intermediate ice volume at which global climate is unstable; upon either reducing or increasing global ice volume, the climate system is stabilized and DO events become infrequent. Instead, our hypothesis suggest that this Goldilocks zone represents a regime of intermediate stability of the interstadial AMOC mode (Figure 4b). It is precisely this intermediate stability regime that allows for a rapid succession of DO events, as the interstadial phases are of short duration yet DO events still occur reliably.

The ice-volume hypothesis has been supported using a three-box model of the North Atlantic ocean, in which the hydrological freshwater flux from the middle to high latitudes was made to increase linearly with growing global ice volume [*Sima et al.*, 2004]. This assumption is at odds with the basic thermodynamic Clausius-Clapeyron relation, evidence for a weakened hydrological cycle during glacial times [*Yung et al.*, 1996], and modern observations that suggest an amplification of the global hydrological cycle under the current warming [*Durack and Wijffels*, 2010]. Furthermore, experiments with fully coupled ocean-atmosphere general circulation models (GCMs) consistently show that the orographic effect of NH ice buildup is to strengthen the AMOC [*Zhu et al.*, 2014; *Zhang et al.*, 2014; *Ullman et al.*, 2014], while the ice-volume hypothesis requires the opposite effect to hold. As such, we deem that to date no strong evidence exists for the correctness of the ice-volume hypothesis.

## 3. Southern Hemisphere Controls on AMOC Stability

The Atlantic surface and intermediate waters that comprise the northward branch of the AMOC enter the South Atlantic from the Pacific via the Drake Passage (including Antarctic Intermediate Water and Subantarctic Mode Water) and from the Indian Ocean via Agulhas Leakage (AL, Figure 5); these two pathways are referred to as the cold- and warm-water route, respectively [*de Ruijter et al.*, 1999; *Talley*, 2013]. Much of the deep water formed in the North Atlantic is ultimately returned to the SO via wind-driven isopycnal upwelling [*Toggweiler and Samuels*, 1995; *Marshall and Speer*, 2012; *Kuhlbrodt et al.*, 2007]. The AMOC is thus fundamentally linked to the global overturning circulation via the SO. Here we will briefly review several processes through which SH climate can influence AMOC strength and stability, as well as proxy evidence that suggests these mechanisms indeed operated in the past.

### 3.1. Bipolar Seesaw in Deep Water Formation

The abyssal oceans fill up with the densest waters, which are formed exclusively in the cold polar regions. A reduction in AABW formation will promote NADW formation and vice versa, resulting in a deep water "seesaw"

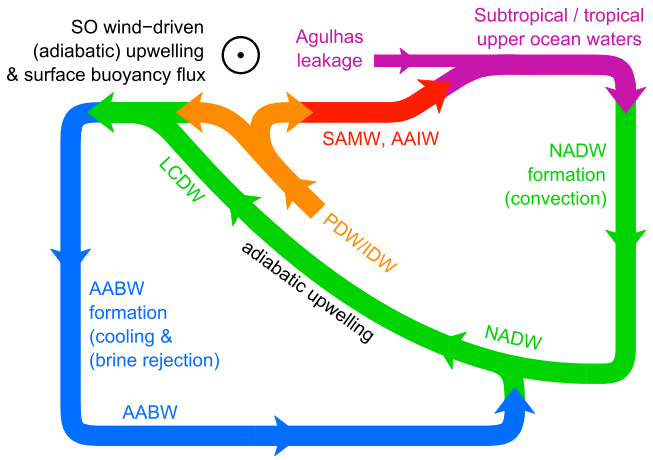


**Figure 5.** Schematic representation of present-day AMOC, redrawn from *Talley* [2013]. Abbreviations are Antarctic Bottom Water (AABW), Antarctic Intermediate Water (AAIW), Subantarctic Mode Water (SAMW), Pacific Deep Water (PDW), Indian Deep Water (IDW), and North Atlantic Deep water (NADW). IDW and PDW are formed through internal diapycnal transformation of AABW (not shown). In the SO, the lighter, low-oxygen IDW/PDW upwells above and north of the denser, saltier NADW [*Talley*, 2013].

[*Broecker*, 1998; *Broecker et al.*, 1999; *Seidov et al.*, 2001; *Fieg and Gerdes*, 2001; *Piotrowski et al.*, 2008]. In simplified terms, one can think of the deep water seesaw as a competition between both polar regions to produce the densest waters. All other things being equal, warming the SH high latitudes will reduce AABW formation by both deep convection and brine rejection. Recent observations indeed suggest that AABW formation has reduced in recent decades, possibly due to warming and freshening of the SH high-latitude oceans [*Azaneu et al.*, 2013; *Purkey and Johnson*, 2012].

### 3.2. Meridional Density/Pressure Gradients

Model analyses suggest links between meridional density (or pressure) gradients and the AMOC strength [e.g., *Hughes and Weaver*, 1994; *Saenko et al.*, 2003], and many box models assume that the density difference between the South Atlantic and the North Atlantic drives the AMOC [e.g., *Rahmstorf*, 1996; *Kuhlbrodt et al.*, 2007]. Decreasing densities of Antarctic Intermediate Water or Subantarctic Mode Water through either warming or freshening can increase the AMOC, either by changing the freshwater fluxes due to the overturning circulation in the South Atlantic associated with AAIW [*Saenko et al.*, 2003] or by increasing the meridional pressure gradient between the South Atlantic and the North Atlantic [*Hughes and Weaver*, 1994], or both. Warming the SH via the thermal bipolar seesaw will increase the meridional density gradient in the Atlantic, which drives a stronger AMOC.

### 3.3. Agulhas Leakage

Transport of salty, warm Indian Ocean surface waters into the South Atlantic across the southern tip of the African continent (Agulhas Leakage) provides an important source of (negative) buoyancy forcing to the AMOC [*de Ruijter et al.*, 1999; *Beal et al.*, 2011]. It has been suggested that the position of the subtropical front may act as a valve (or "gatekeeper") of the AL [*Bard and Rickaby*, 2009]; during glacial climates, this front migrates northward, thereby reducing AL. Meridional migration of the subtropical front is associated with a similar movement of the SH westerly winds [*De Boer et al.*, 2013]. Climate model experiments that impose a northward shift in the SH westerlies find a reduction in AMOC strength by a reduction in the AL [*Sijp and England*, 2008, 2009]. *Peeters et al.* [2004] have reconstructed past strength of the Indian-Atlantic exchange using planktic foraminiferal assemblages. They observe enhanced Agulhas Leakage fauna during all interglacial stages, which is indicative of increased AL and consistent with a southernmost position of the subtropical front/SH westerlies during these periods. Conversely, during glacial stages AL is low. More recently, *Marino et al.* [2013] have used paired Mg/Ca-$\delta^{18}$O data to reconstruct AL on millennial timescales; their record shows increased AL in parallel with Antarctic warm events (AIM events), as well as in response to prominent NH Heinrich events.

### 3.4. Wind-Driven Upwelling in the SO

NADW outcrops (primarily) in the Southern Ocean through wind-driven isopycnal upwelling (Figure 5), and this return flow is important in maintaining the strength and stability of the AMOC [*Toggweiler and Samuels*, 1995; *Marshall and Speer*, 2012]. Variations in the position and/or strength of the westerlies are thought to control SO upwelling on these timescales [*Anderson et al.*, 2009; *Toggweiler et al.*, 2006]. This notion is supported by climate model experiments forced with a latitudinal displacement of the SH westerlies, which suggest that a northward (southward) displacement leads to reduced (increased) SO upwelling and reduced (increased) formation of deep water in the North Atlantic [*Toggweiler and Samuels*, 1995; *Völker and Köhler*, 2013]—it must be noted that the response to SO wind stress changes is typically attenuated in eddy-resolving ocean models [*Hallberg and Gnanadesikan*, 2006]. It has been suggested that the opal (biogenic silica) flux to SO sediments can be used as a proxy for upwelling [*Anderson et al.*, 2009]. The opal burial rate shows clear millennial-scale variations that, within dating uncertainty, are correlated with SH high-latitude temperature (Figure 1f).

These four mechanisms can roughly be divided into thermal effects (deep water seesaw and density gradients) and wind effects (Agulhas Leakage and SO upwelling). While we have good proxy reconstructions for past temperatures, scientific understanding of past strength and position of the SH westerlies is still very much incomplete. It is generally believed that during the LGM the SH westerlies were displaced equatorward, and while this hypothesis is consistent with the majority of available proxy evidence, other scenarios cannot be fully excluded [*Kohfeld et al.*, 2013]. Moreover, climate models do not consistently simulate the northward displacement during the LGM [*Sime et al.*, 2013; *Rojas et al.*, 2009]. In response to the present global warming, both observations and models consistently suggest a poleward displacement and strengthening of the SH westerlies corresponding to a persistent positive index of the Southern Annular Mode, although much of the observed response to date is due to the depletion of stratospheric ozone [*Kushner et al.*, 2001; *Thompson and Solomon*, 2002; *Yin*, 2005; *Fyfe and Saenko*, 2006]. *Sikes et al.* [2009] tracked latitudinal movement of the subtropical front in the Australian sector of the SO—displacement of which is directly linked to displacement of the westerlies [*De Boer et al.*, 2013]. They find that the subtropical front/westerlies were in their most southerly position during the warmth of MIS 5 (~2°C higher SST than present day, in their records), a relatively northerly position during the MIS 3 and MIS 4 cool periods, and in their northernmost position during the LGM.

SH warmth thus appears to be associated with poleward movement and/or strengthening of the SH westerlies. This relationship implies that the thermal effects and wind effects amplify one another with respect to their influence on the AMOC strength, as we shall show in the next section.

## 4. Climate Model Experiments of Warming the Southern Ocean

### 4.1. Experimental Setup

To test our hypothesis, we performed a series of model experiments using the University of Victoria (UVic) Earth System Climate Model of intermediate complexity [*Weaver et al.*, 2001] version 2.9 [*Eby et al.*, 2009]. The UVic model consists of a global three-dimensional ocean general circulation model at coarse resolution (1.8°latitude × 3.6°longitude, 19 vertical levels), a one-layer atmospheric energy-moisture balance model, a dynamic/thermodynamic sea ice model, and land and ocean biogeochemical components. The simplified atmospheric model uses prescribed fields for wind stress, moisture advection velocities, and cloud albedo diagnosed from modern estimates [*Kalnay et al.*, 1996]. LGM simulations include reconstructed ice sheets [*Peltier*, 1994], reduced atmospheric $CO_2$ levels (190 ppm), and wind stress anomalies as simulated by the PMIP3 models [*Braconnot et al.*, 2012].

Starting from both LGM and preindustrial (PI) background conditions, we apply an additional heat flux $\Phi$ to the latitudinal band of the SO in order to selectively cool or warm the SO (Figure 6a). We use five different $\Phi$ scenarios ($\Phi = -4, -2, +4, +8$, and $+12$ W m$^{-2}$) and a control run ($\Phi = 0$) and integrate for 2500 years to let the model approach equilibrium. Note that the color coding of Figure 6a is used throughout Figures 6 and 7.

For completeness, we have furthermore performed a model experiment under LGM background conditions ($\Phi = 0$), in which we have increased the strength of the SH westerlies. In the 40°–60°S latitudinal band, we amplify the wind stress by 25%. This model run is also spun up for 2500 years. The response of the ocean circulation to strengthening and/or shifting the SH westerlies has been studied in great detail elsewhere [e.g., *Toggweiler and Samuels*, 1995; *Rahmstorf and England*, 1997; *Brix and Gerdes*, 2003; *Sijp and England*, 2009], and we will discuss these simulations only briefly. Moreover, we aim to understand the correlation between

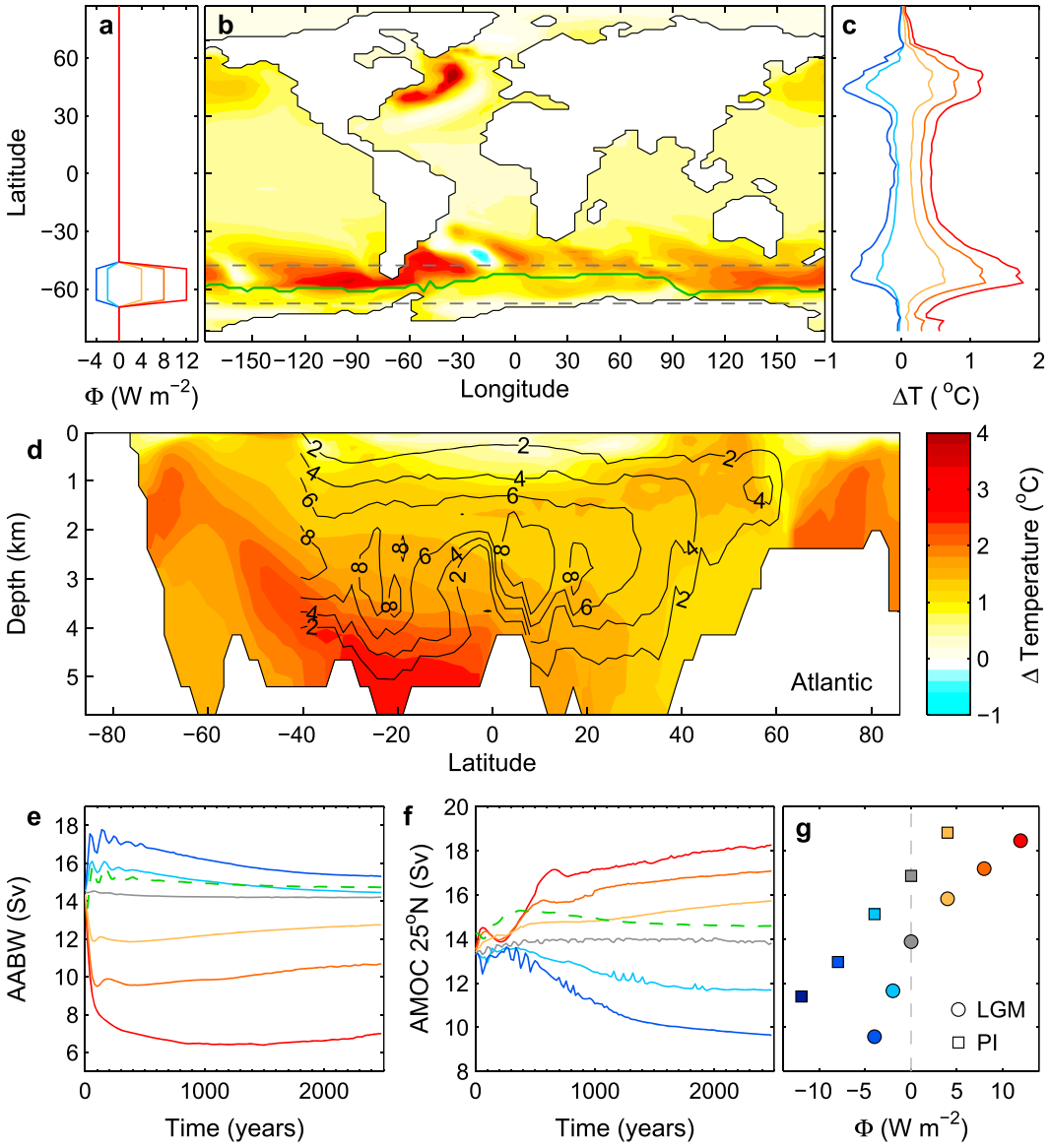


**Figure 6.** UVic model forcing and response for LGM background conditions (annual mean values). (a) Surface radiative forcing function Φ; same color coding is used for all panels. (b) SST anomaly after 2500 years of model integration for $\Phi = +12$ W m$^{-2}$. Boundary of seasonal sea ice (contour of 10% annual mean cover) shown by green line. (c) Zonally averaged SST anomaly. (d) Atlantic temperature and stream function anomaly (in sverdrup, Sv) after 2500 years of model integration for $\Phi = +12$ W m$^{-2}$. For Figures 6b through 6d, the climate anomalies are calculated by subtracting the control run. (e) AABW response in Sv (1 Sv = $10^6$ m$^3$s$^{-1}$), calculated from the global stream function. Dashed green line in Figures 6e and 6f shows simulation with 25% stronger SH westerlies. (f) AMOC strength is in Sv, evaluated as the maximum of the Atlantic stream function at 25°N. (g) Equilibrium AMOC strength as a function of the applied forcing Φ from both LGM and PI background climates; *y* axis is identical to Figure 6f.

interstadial duration and SH high-latitude temperature (Figure 2); and therefore, the SO warming/cooling scenarios provide a more direct comparison.

### 4.2. Model Response to SO Warming/Cooling

The simulated SST anomaly after 2500 years of model integration (using $\Phi = +12$ W m$^{-2}$) is shown in Figure 6b. As expected, strong surface warming is seen in the SO latitudes; areas of the SO covered by seasonal sea ice (green line) are insulated from the heat flux Φ for at least part of the year and have a more muted temperature response. Strong warming also occurs in the SH abyssal ocean (Figure 6d). Surprisingly, warming is also simulated in the northwest Atlantic, although no forcing was applied there. This warming is due to increased

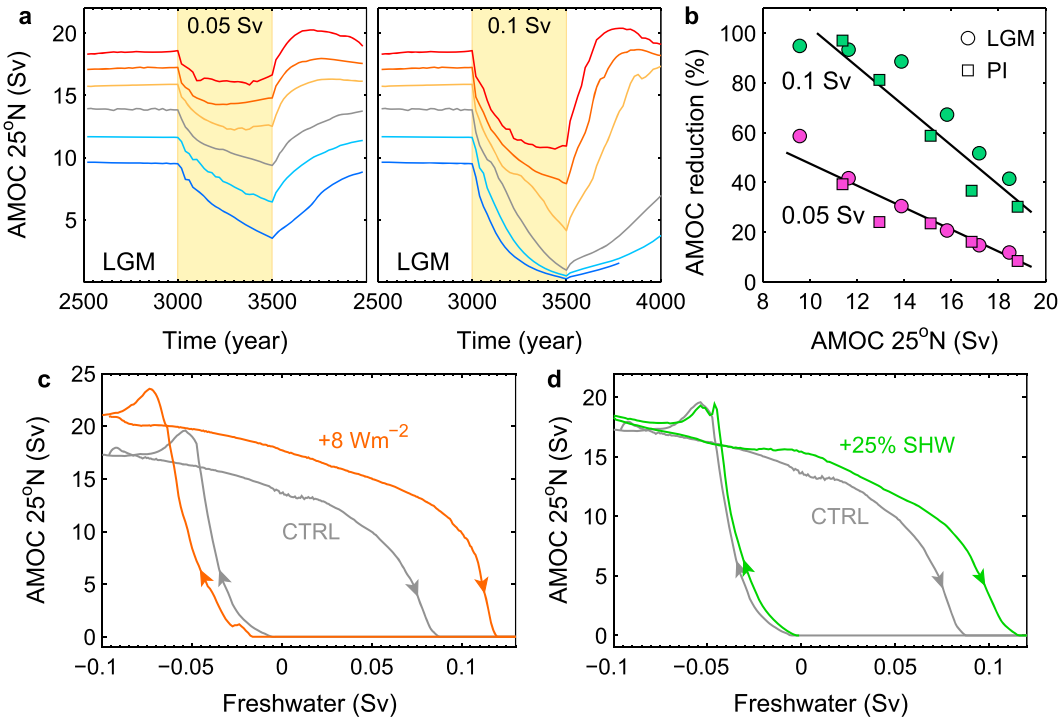


**Figure 7.** AMOC sensitivity to freshwater forcing in the UVic model. (a) AMOC response to 0.05 and 0.1 Sv North Atlantic freshwater flux for LGM background climate, and different values of Φ (color coded as in Figure 6). (b) AMOC reduction for 0.05 and 0.1 Sv experiments and both PI and LGM background climates; the reduction is calculated by subtracting the AMOC strength in the $t = 3400$ to $t = 3500$ interval from the equilibrium strength and dividing by the equilibrium strength. (c) AMOC stability diagram for $\Phi = 0$ (grey) and $\Phi = +8$ W m$^{-2}$ (orange). From an initial freshwater flux of −0.1 Sv, we increase the flux at a rate of $5 \times 10^{-2}$ Sv ka$^{-1}$; once the AMOC has collapsed, the freshwater flux is decreased at the same rate as before. The arrows mark the direction in which the hysteresis is traversed. (d) AMOC stability diagram from control run (grey) and a scenario in which the strength of the SH westerlies has been increased by 25% (green); both scenarios use $\Phi = 0$.

northward heat transport by an invigorated AMOC, as described below. The zonally integrated SST anomaly suggests that the temperature response scales approximately linearly with the applied forcing (Figure 6c).

Upon warming the SO, we observe an immediate reduction in AABW formation (Figure 6e), and vice versa, cooling the SO strengthens AABW formation. The AMOC response is delayed and more gradual, taking around 2000 years to fully develop (Figure 6f). The stream function anomaly (for $\Phi = +12$ W m$^{-2}$) in the Atlantic after 2500 years indicates a strengthening and deepening of the middepth overturning cell associated with NADW, and a compression and weakening of the bottom overturning cell associated with reduced penetration of AABW into the Atlantic (Figure 6d). The changes in AABW and NADW formation are opposite in all the heat flux simulations, displaying the deep water seesaw effect. The equilibrium AMOC strength (starting from both LGM and PI background conditions) increases as a function of the heat flux anomaly Φ (Figure 6g); we find a clear monotonic (albeit, at least for the LGM case, nonlinear) relationship between the applied SO warming and the simulated AMOC strength.

The initial increase in AMOC strength upon SO warming correlates well with an increase in the north-south density contrast in the Atlantic (supporting information); however, this correlation breaks down after model year $t \approx 800$ when the density contrast decreases again, while the AMOC strength continues to rise (Figure 6f). It is around this time that the reduced formation of AABW has led to a reduction in the density stratification of the North Atlantic, which in turn promotes NADW formation. These simulations thus suggest a two-stage intensification of the AMOC strength: an initial "push" due to an increase in the Atlantic meridional density gradient of upper and intermediate waters, followed by a "pull" from the deep ocean via the deep water seesaw.

The applied SO high-latitude warming reduces the meridional density (or pressure) gradient in the SH oceans, which results in a weakening of the ACC following the principle of geostrophy. We further observe an atten-

dant equatorward shift of the ACC and of the southern boundary of the South Atlantic Gyre (explaining the cooling anomaly seen there in Figure 6b). A more detailed analysis of the oceanic response to SO warming is provided in the supporting information.

### 4.3. Testing the AMOC Stability

Next, we investigate the stability of the AMOC using freshwater fluxes applied to the North Atlantic. We acknowledge that many other mechanisms may be responsible for DO variability. However, freshwater forcing (or hosing) provides a robust and well-documented strategy for AMOC destabilization [*Kageyama et al.*, 2010]. We suggest that the response to freshwater provides a quantitative measure of AMOC stability, i.e., its sensitivity to perturbations. An overturning that is sensitive to freshwater forcing is probably sensitive to perturbations of a different nature also.

Extending onto our 2500 yearlong spin-up runs, we apply a freshwater pulse of 500 year duration starting at $t = 3000$ (Figure 7a). We tested 0.05 and 0.1 Sv freshwater forcings for all the different values of $\Phi$. In all these experiments, the freshwater-induced AMOC reduction is smallest when the SO is warmest (and the AMOC is strongest). For example, consider the 0.05 Sv forcing at LGM background conditions (Figure 7a, left). For the $\Phi = +12$ W m$^{-2}$ case (upper, dark red curve), a 2.5 Sv AMOC reduction is induced; for the $\Phi = -4$ W m$^{-2}$ case (lowest, dark blue curve) the same freshwater forcing induces a 6 Sv AMOC reduction. The observed AMOC reductions are summarized in Figure 7b, where we combine results from the LGM (squares) and PI (circles) runs. The UVic simulations suggest that the AMOC strength itself is the best predictor for the AMOC stability. Overall, the simulations with a warmer SO have a stronger AMOC and are thus less sensitive to perturbations.

In Figure 7c we show the AMOC stability diagrams for $\Phi = 0$ (grey) and $\Phi = +8$ W m$^{-2}$ (orange), which all show the familiar hysteresis loop as a function of freshwater forcing [e.g., *Rahmstorf*, 1996]. Details are given in the figure caption. We find that application of a $\Phi = +8$ W m$^{-2}$ SO heat flux anomaly shifts the stability of the vigorous (interstadial) AMOC mode to the right relative to the control run (grey), i.e., toward larger freshwater fluxes. By warming the SO, we have thus made the AMOC more tolerant of freshwater and raised the threshold for AMOC collapse. The effect of SO warming on the collapsed AMOC mode is opposite (i.e., a shift to lower freshwater values) and of a smaller magnitude.

In the simulations with 25% increased SH westerly wind stress, the AMOC increases by ~1 Sv in response to the applied wind forcing (Figure 6f, dashed green line). The AMOC stability diagram for this model configuration is shown in Figure 7d. We find that strengthening the SH westerlies has a comparable influence on the stability diagram as warming the SO, namely it shifts the stability of the vigorous AMOC mode toward larger freshwater fluxes. The stability of the collapsed AMOC mode appears to be unaffected by changes in the wind stress.

## 5. Discussion

### 5.1. Model Results Discussion

The main objective of these model experiments is to investigate the influence of SO warmth on the strength and stability of the AMOC. We find that equilibrium AMOC strength consistently increases with SO temperature, both under LGM and preindustrial background conditions (Figure 6g). We further find that with increasing SO warmth, the AMOC becomes less susceptible to destabilization by freshwater addition to the North Atlantic: the AMOC response to 500 yr duration freshwater pulses is reduced (Figures 7a and 7b), and the freshwater threshold for AMOC collapse is increased (Figure 7c). These two different ways of testing the response to freshwater forcing are of course closely related—due to the highly nonlinear shape of the AMOC-freshwater curve, the AMOC response to a pulse of freshwater will be larger as one is closer to the threshold.

These model simulations support our interpretation of the observed correlation between interstadial duration and SH high-latitude temperature (Figure 2). During periods of SH high-latitude warmth, the AMOC is more stable and therefore less likely to collapse; this in turn allows the vigorous, interstadial AMOC mode to persist for longer periods of time. In our simulations, we vary Southern Ocean SST over a range of ~2.5°C (Figure 6c), which is a conservative range given that reconstructions suggest glacial-interglacial changes of ~6°C or larger [*Barrows et al.*, 2007; *Lopes Dos Santos et al.*, 2012].

As discussed in section 3, SH warming is expected to be accompanied by a strengthening and/or poleward displacement of the SH westerlies. We find that intensifying the SH westerlies' wind stress by 25% leads to a minor increase in equilibrium AMOC strength, as well as an increased threshold for meltwater-induced collapse

(Figure 7d). The effects of temperature and wind stress on the strength and stability of the AMOC are thus complementary in our simulations. Upon increasing the SO wind stress, we furthermore enhance AABW formation (Figure 7e)—this result is in agreement with prior studies that likewise find that deep water production in both hemispheres is similarly affected by SO wind stress anomalies [*Brix and Gerdes*, 2003]. However, the magnitude of the wind stress anomaly we apply is probably rather large. To achieve a 25% increase in the SH wind stress, GCMs typically need to be forced quite severely, for example, through a 120 W $m^{-2}$ cooling flux to the North Atlantic [*Lee et al.*, 2011] or through the removal of the entire Antarctic ice sheet [*Schmittner et al.*, 2011]. PMIP2 model simulations suggest a glacial-interglacial change in wind stress that is less than the 25% applied here [*Rojas et al.*, 2009], and the same is true in the PMIP3 simulations (J. Muglia, personal communication 2015). These simulations should thus be viewed as a sensitivity experiment, rather than a simulation of past conditions.

The simulations with an applied SO heat flux $\Phi$ allow us to study the thermal controls on AMOC strength, namely the deep water seesaw and the meridional density gradient (section 3). We find both effects to be important but on different timescales (supporting information). The north-south density contrast in the surface Atlantic responds quickly to the applied heat flux anomaly, and an increased (reduced) density contrast appears to drive the initial AMOC increase (decrease) upon warming (cooling) the SO. The deep water seesaw, on the other hand, operates on multicentennial to millennial timescales. While the rate of AABW formation responds quickly (decadal timescales) to the applied heat flux anomaly, it takes many centuries for the density anomaly to spread to the abyssal and deep waters of the Atlantic where it can affect the rate of NADW formation.

The simulation with 25% increased SH westerly wind stress (Figure 7d) allows us to study the wind controls on AMOC strength, namely the wind-driven SO upwelling and the Agulhas Leakage. We find in our simulations that both are simultaneously affected. In response to the wind stress anomaly, the model simulates an increase in SO upwelling from 21.1 to 25.2 Sv and an increase in AL from 4.5 to 8.1 Sv (values that are roughly in line with poorly constrained present-day estimates of 2 to 15 Sv) [*Beal et al.*, 2011]. Figure 7d thus represents the aggregate effect of increasing both upwelling and AL. In the thermally forced simulations, equilibrium AL and SO upwelling did not change appreciably in response to $\Phi$—we do observe a temporary increase in AL upon warming the SO, which has disappeared by $t = 2500$ (supporting information).

We therefore conclude that between the different model experiments, we test and validate all four mechanisms of SO control identified in section 3, although we cannot disentangle the effects of Agulhas Leakage and wind-driven upwelling. Application of a $\Phi = +8$ W $m^{-2}$ heat flux anomaly shifts the vigorous AMOC branch in the freshwater stability diagram by about the same amount as a 25% wind stress anomaly does (Figures 7c and 7d). And while the induced SO temperature changes are within the range suggested by proxy-based SST reconstructions, the SH wind stress anomaly we apply is probably unrealistically large (as argued above). Moreover, the wind stress response is expected to be muted in eddy-resolving models [*Hallberg and Gnanadesikan*, 2006]. Combined, this suggests that the thermal effects may be more important than the wind effects in their respective control on AMOC strength and stability.

So far, we have discussed the behavior of the vigorous AMOC mode; we now turn to the collapsed or AMOC "off" mode of the stability diagrams. In general, we find a much stronger influence of SH climate on the vigorous AMOC mode than on the collapsed mode, both in thermally forced (Figure 7c) and wind-forced simulations (Figure 7d). This is in line with our observation that interstadial duration is strongly correlated with Antarctic temperature ($r = 0.92$; Figure 2), and stadial duration only very weakly ($r = -0.28$; Figure 3).

In these simulations, warming the SO increases the stability of both the vigorous and the collapsed modes, as reflected by a widening of the hysteresis loop (Figure 7c). Based on these simulations, one would thus expect stadial durations to increase with warmer SH conditions. This is indeed the case when comparing MIS 3 and MIS 5, where the latter, warmer period has slightly longer stadial durations on average. However, this is clearly not true for MIS 2 and MIS 4, which both have long stadial durations during cold SH conditions. The model simulations thus suggest that the long stadial durations seen during MIS 2 and MIS 4 likely reflect the absence of DO events, rather than an increased stability of the stadial AMOC mode.

It is conceivable that the off mode in the stability diagrams corresponds to the (meltwater induced) Heinrich AMOC mode, rather than to the stadial mode. For example, during the stadial climate of the LGM the Atlantic

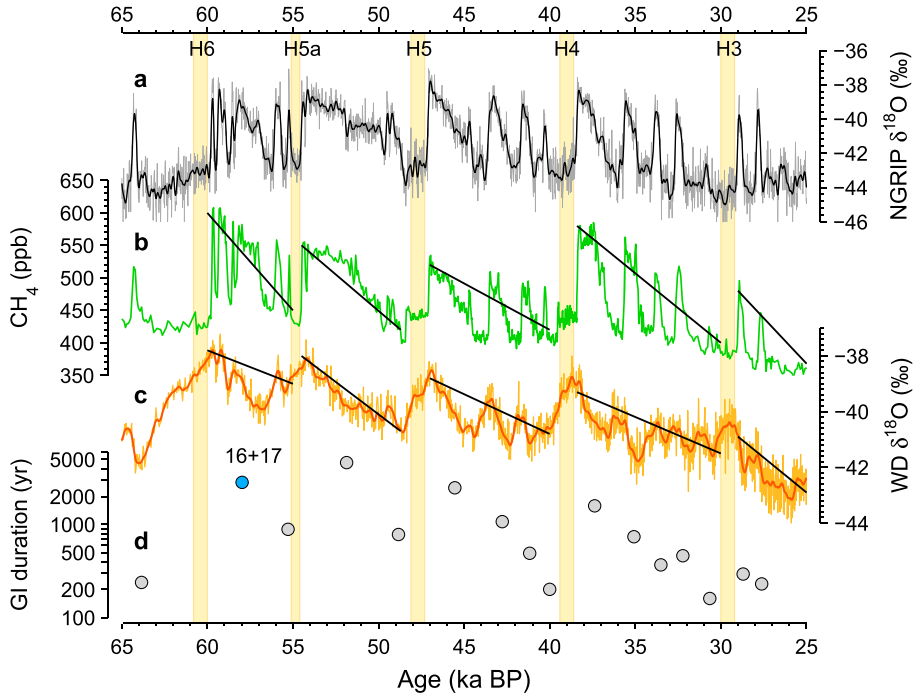


**Figure 8.** Bond cycles of MIS 3. (a) NGRIP $\delta^{18}$O as a proxy for Greenland temperature. (b) Atmospheric methane from the WAIS Divide ice core [*WAIS Divide Project Members*, 2015]. (c) WAIS Divide $\delta^{18}$O as a proxy for SH high-latitude temperature. (d) Greenland interstadial duration. Vertical yellow bars denote Heinrich stadials H3 through H6. As in Figure 2, treating the subevents that make up DO 16 and 17 as a single event provides a greatly improved agreement with the general pattern. These subevents are separated by stadials of unusually short duration, which may reflect meltwater incursions as the NH ice sheets are retreating from their MIS 4 highstand.

overturning is thought to have been quite strong [e.g *McManus et al.*, 2004]. The shifts observed in the off branch of the stability diagram may thus be of limited value in interpreting the correlation between SH climate and stadial duration.

In these experiments, SO warmth is controlled through the heat flux $\Phi$. Future experiments could investigate the relationship between AMOC stability and SO warmth using a series of time slices throughout the last glacial period, in which orbital configuration, atmospheric greenhouse gases, and ice sheet topography are simultaneously altered. The advantage of the heat flux approach taken here is that it allows us to study the influence of SO warmth in isolation; the advantage of the time slice approach is that it simulates past climatic conditions more realistically. It will furthermore be valuable to repeat these simulations in a coupled ocean-atmosphere GCM to allow the SH wind field to respond dynamically to increased SO warmth.

### 5.2. Bond Cycles

It has been observed that DO events are grouped in so-called Bond cycles of ~7 ka duration, which are separated by Heinrich events [*Bond et al.*, 1993; *Lehman*, 1993]. Within each cycle, the duration and magnitude of successive interstadial events decrease (Figure 8). Iceberg delivered freshwater during H events can suppress NADW formation and lengthen stadial duration, allowing heat to accumulate in the SH via the thermal bipolar seesaw [*Stocker and Johnsen*, 2003; *EPICA Community Members*, 2006]. The first DO event of a Bond cycle thus occurs at relatively warm SH high-latitude conditions, which we suggest leads to a more stable AMOC and a long interstadial duration. During the Bond cycle, SH heat is lost to the NH via the seesaw mechanism (Figure 8c); and therefore, successive DO events happen at progressively colder SH conditions. Our hypothesis implies that the gradual cooling of the SH throughout each Bond cycle results in a progressive shortening of DO interstadial durations, as is indeed observed (Figure 8d). Our hypothesis thus provides a straightforward and self-consistent explanation for the diminishing duration of DO interstadials within each Bond cycle.

In dynamical systems, oscillatory behavior signifies the dominance of negative feedbacks. Unless the DO cycle is periodically forced (as in, e.g., *Ganopolski and Rahmstorf* [2001]), negative feedbacks of some form

are required to sustain the DO oscillation. Our hypothesis provides one such negative feedback. During interstadial periods, the SO cools via the thermal bipolar seesaw, which reduces the stability of the interstadial AMOC mode itself, expediting its collapse. And vice versa, during stadial periods the SO warms, which then restores the stability of the interstadial mode. In this perspective, the Bond cycle could perhaps be viewed as a damped oscillator: the large amount of excess SH heat that accumulates during Heinrich stadials is reduced through a series of DO oscillations of diminishing amplitude and interstadial duration, a pattern resembling the behavior of a weakly damped oscillator.

### 5.3. Future AMOC Evolution

Our hypothesis may have implications for the fate of the AMOC under future global warming from anthropogenic $CO_2$ emissions. Climate model simulations consistently suggest an initial (transient) AMOC weakening associated with increased North Atlantic stratification from surface warming and freshening [*Intergovernmental Panel on Climate Change (IPCC)*, 2013; *Kuhlbrodt et al.*, 2009], yet great uncertainty remains regarding its long-term evolution. The latest Intergovernmental Panel on Climate Change report (Fifth Assessment Report) notes that "a collapse beyond the 21st century for large sustained warming cannot be excluded," and the report assigns low confidence to our current understanding of AMOC evolution beyond the 21st century [*IPCC*, 2013]. The paleo-observations show that in a warmer world interstadial durations are longer (Figure 2), which we here interpret as evidence for a stronger and more stable AMOC overturning. As such, our hypothesis, if correct, would predict a long-term increase in equilibrium AMOC strength under future anthropogenic global warming [see also *Toggweiler and Russell*, 2008]. Indeed, recent observations suggest a reduction in AABW volume [*Purkey and Johnson*, 2012; *Azaneu et al.*, 2013], an increase in Agulhas Leakage [*Biastoch et al.*, 2009], and an increase in Atlantic salinity [*Durack and Wijffels*, 2010]; all of which should act to stabilize and strengthen the AMOC, yet observations show that the AMOC is currently weakening [*Srokosz and Bryden*, 2015]. The future evolution of the AMOC may thus depend on the competition between a short-term, transient weakening driven by North Atlantic surface warming/freshening, and a long-term increase in equilibrium strength driven by circulation changes of the Southern Ocean.

## 6. Summary and Conclusions

We have shown that Dansgaard-Oeschger interstadial durations are strongly correlated with Antarctic temperatures (Figure 2), with long (short) interstadials occurring during times of SH warmth (cold). During the coldest periods (MIS 2 and MIS 4) DO events are (nearly) absent, resulting in long stadial periods; for all other periods, there is no strong correlation between stadial duration and Antarctic temperature (Figure 3). Combined, this leads to maximum DO activity (shortest DO recurrence times) during periods of intermediate SH high-latitude temperatures, such as during MIS 3 (Figure 4).

We propose that the timing characteristics of the DO cycles are controlled by SH climate through the influence of Southern Ocean processes on the strength and stability of the AMOC. During periods of SH high-latitude warmth, the vigorous, interstadial AMOC mode is more stable, which is reflected by long interstadial durations.

We identify four mechanisms through which SH climate can exert the proposed influence on AMOC strength and stability: (i) the rate of AABW formation and the "deep water seesaw," (ii) the Atlantic density/pressure gradients that drive the AMOC, (iii) buoyancy forcing by transport of warm, saline Indian Ocean surface waters across the southern tip of Africa (Agulhas Leakage), and (iv) SO wind-driven upwelling of deep waters. Proxy evidence supports the idea that both SO upwelling and Agulhas Leakage are enhanced during periods of SH high-latitude warmth.

We present climate model experiments using an Earth system model of intermediate complexity. We find that warming (cooling) the latitudinal band of the SO reduces (enhances) AABW formation around Antarctica, which in turn leads to a strengthening (weakening) of the AMOC via the deep water seesaw (Figure 6). In our simulations, SO warmth raises the threshold for freshwater-induced AMOC collapse and makes the AMOC less susceptible to freshwater pulses into the North Atlantic (Figure 7). Strengthening the SH westerly winds likewise increases the AMOC strength and stability. Combined, these experiments confirm that under warm SO conditions the vigorous, interstadial AMOC mode is less susceptible to perturbations, which allows it to persist for longer periods of time, resulting in a long DO interstadial duration.

Our hypothesis can provide a straightforward explanation for the observation that within each ~7 ka Bond cycle the duration of successive DO events decreases (Figure 8); it provides a possible negative feedback required to sustain DO oscillations; it suggests an influence of long-term (i.e., orbital scale) variations in background climate on the timing characteristics of the DO cycle; and it may have consequences for the future evolution of the AMOC under anthropogenic global warming.

**Acknowledgments**
We want to thank Ed Brook, Feng He, Jeff Severinghaus, Alan Mix, Dave Ullman, Brad Markle, and Shaun Marcott for support and/or fruitful discussions. All paleoclimate data used in this work are publicly available with their original publications as cited in the figure captions. Data can be obtained via http://dx.doi.org/10.1038/nature14401 (WAIS $\delta^{18}O$ and $CH_4$), http://dx.doi.org/10.1126/science.1226368 (Antarctic Temperature Stack), or through the NOAA climatic data center at http://www.ncdc.noaa.gov/paleo/ (all other data). The code of the UVic climate model is available at http://climate.uvic.ca/model/2.9/. Requests for materials or information should be addressed to Christo Buizert (buizertc@science.oregonstate.edu). We acknowledge funding through the NOAA Climate and Global Change postdoctoral fellowship program, administered by the University Corporation for Atmospheric Research (to C.B.) and through NSF grants from the Marine Geology and Geophysics Program (OCE-1131834; to A.S.).

## References

Alley, R. B., S. Anandakrishnan, P. Jung, and A. Clough (2001), Stochastic resonance in the North Atlantic: Further insights, in *The Oceans and Rapid Climate Change*, pp. 57–68, AGU, Washington, D. C.

Anderson, R. F., S. Ali, L. I. Bradtmiller, S. H. H. Nielsen, M. Q. Fleisher, B. E. Anderson, and L. H. Burckle (2009), Wind-driven upwelling in the Southern Ocean and the deglacial rise in atmospheric $CO_2$, *Science*, *323*(5920), 1443–1448, doi:10.1126/science.1167441.

Azaneu, M., R. Kerr, M. M. Mata, and C. A. E. Garcia (2013), Trends in the deep Southern Ocean (1958–2010): Implications for Antarctic bottom water properties and volume export, *J. Geophys. Res. Oceans*, *118*, 4213–4227, doi:10.1002/jgrc.20303.

Banderas, R., et al. (2012), Role of $CO_2$ and Southern Ocean winds in glacial abrupt climate change, *Clim. Past*, *8*, 1011–1021.

Banderas, R., J. Alvarez-Solas, A. Robinson, and M. Montoya (2014), An interhemispheric mechanism for glacial abrupt climate change, *Clim. Dyn.*, *44*, 2897–2908, doi:10.1007/s00382-014-2211-8.

Bard, E., and R. E. M. Rickaby (2009), Migration of the subtropical front as a modulator of glacial climate, *Nature*, *460*(7253), 380–383.

Barker, S., P. Diz, M. J. Vautravers, J. Pike, G. Knorr, I. R. Hall, and W. S. Broecker (2009), Interhemispheric Atlantic seesaw response during the last deglaciation, *Nature*, *457*(7233), 1097–1102, doi:10.1038/nature07770.

Barrows, T. T., S. Juggins, P. De Deckker, E. Calvo, and C. Pelejero (2007), Long-term sea surface temperature and climate change in the Australian-New Zealand region, *Paleoceanography*, *22*, PA22215, doi:10.1029/2006PA001328.

Beal, L. M., W. P. M. De Ruijter, A. Biastoch, and R. Zahn (2011), On the role of the Agulhas system in ocean circulation and climate, *Nature*, *472*(7344), 429–436.

Bereiter, B., S. Eggleston, J. Schmitt, C. Nehrbass-Ahles, T. F. Stocker, H. Fischer, S. Kipfstuhl, and J. Chappellaz (2015), Revision of the EPICA Dome C $CO_2$ record from 800 to 600 kyr before present, *Geophys. Res. Lett.*, *42*, 542–549, doi:10.1002/2014GL061957.

Biastoch, A., C. W. Böning, F. U. Schwarzkopf, and J. R. E. Lutjeharms (2009), Increase in Agulhas Leakage due to poleward shift of Southern Hemisphere westerlies, *Nature*, *462*(7272), 495–498, doi:10.1038/nature08519.

Böhm, E., J. Lippold, M. Gutjahr, M. Frank, P. Blaser, B. Antz, J. Fohlmeister, N. Frank, M. Andersen, and M. Deininger (2015), Strong and deep atlantic meridional overturning circulation during the last glacial cycle, *Nature*, *517*(7532), 73–76.

Bond, G., W. Broecker, S. Johnsen, J. McManus, L. Labeyrie, J. Jouzel, and G. Bonani (1993), Correlations between climate records from North Atlantic sediments and Greenland ice, *Nature*, *365*(6442), 143–147.

Braconnot, P., S. P. Harrison, M. Kageyama, P. J. Bartlein, V. Masson-Delmotte, A. Abe-Ouchi, B. Otto-Bliesner, and Y. Zhao (2012), Evaluation of climate models using palaeoclimatic data, *Nat. Clim. Change*, *2*(6), 417–424, doi:10.1038/nclimate1456.

Braun, H., M. Christl, S. Rahmstorf, A. Ganopolski, A. Mangini, C. Kubatzki, K. Roth, and B. Kromer (2005), Possible solar origin of the 1,470-year glacial climate cycle demonstrated in a coupled model, *Nature*, *438*(7065), 208–211.

Braun, H., P. Ditlevsen, J. Kurths, and M. Mudelsee (2011), A two-parameter stochastic process for Dansgaard-Oeschger events, *Paleoceanography*, *26*, PA3214, doi:10.1029/2011PA002140.

Brix, H., and R. Gerdes (2003), North Atlantic deep water and Antarctic bottom water: Their interaction and influence on the variability of the global ocean circulation, *J. Geophys. Res.*, *108*(C2), 3022, doi:10.1029/2002JC001335.

Broecker, W. S. (1998), Paleocean circulation during the last deglaciation: A bipolar seesaw?, *Paleoceanography*, *13*(2), 119–121, doi:10.1029/97PA03707.

Broecker, W. S. (2006), Abrupt climate change revisited, *Global Planet. Change*, *54*(3–4), 211–215, doi:10.1016/j.gloplacha.2006.06.019.

Broecker, W. S., S. Sutherland, and T.-H. Peng (1999), A possible 20th-century slowdown of Southern Ocean deep water formation, *Science*, *286*(5442), 1132–1135.

Buizert, C., et al. (2014), Greenland temperature response to climate forcing during the last deglaciation, *Science*, *345*(6201), 1177–1180, doi:10.1126/science.1254961.

Buizert, C., et al. (2015), The WAIS Divide deep ice core WD2014 chronology—Part 1: Methane synchronization (68–31 ka BP) and the gas age-ice age difference, *Clim. Past*, *11*, 153–173, doi:10.5194/cp-11-153-2015.

Carlson, A. E., and P. U. Clark (2012), Ice sheet sources of sea level rise and freshwater discharge during the last deglaciation, *Rev. Geophys.*, *50*, RG4007, doi:10.1029/2011RG000371.

Clark, P. U., N. G. Pisias, T. F. Stocker, and A. J. Weaver (2002), The role of the thermohaline circulation in abrupt climate change, *Nature*, *415*(6874), 863–869, doi:10.1038/415863a.

Clement, A. C., M. A. Cane, and R. Seager (2001), An orbitally driven tropical source for abrupt climate change, *J. Clim.*, *14*(11), 2369–2375, doi:10.1175/1520-0442(2001)014<2369:aodtsf>2.0.co;2.

Crowley, T. J. (1992), North Atlantic deep water cools the Southern Hemisphere, *Paleoceanography*, *7*(4), 489–497, doi:10.1029/92PA01058.

Curry, W. B., and D. W. Oppo (1997), Synchronous, high-frequency oscillations in tropical sea surface temperatures and North Atlantic deep water production during the last glacial cycle, *Paleoceanography*, *12*(1), 1–14, doi:10.1029/96PA02413.

Dansgaard, W., H. B. Clausen, N. Gundestrup, C. U. Hammer, S. F. Johnsen, P. M. Kristinsdottir, and N. Reeh (1982), A new Greenland deep ice core, *Science*, *218*(4579), 1273–1277, doi:10.1126/science.218.4579.1273.

de Ruijter, W. P. M., A. Biastoch, S. S. Drijfhout, J. R. E. Lutjeharms, R. P. Matano, T. Pichevin, P. J. van Leeuwen, and W. Weijer (1999), Indian-Atlantic interocean exchange: Dynamics, estimation and impact, *J. Geophys. Res.*, *104*, 20,885–20,910, doi:10.1029/1998JC900099.

De Boer, A. M., R. M. Graham, M. D. Thomas, and K. E. Kohfeld (2013), The control of the Southern Hemisphere westerlies on the position of the subtropical front, *J. Geophys. Res. Oceans*, *118*, 5669–5675, doi:10.1002/jgrc.20407.

Ditlevsen, P. D. (1999), Observation of $\alpha$-stable noise induced millennial climate changes from an ice-core record, *Geophys. Res. Lett.*, *26*(10), 1441–1444.

Ditlevsen, P. D., M. S. Kristensen, and K. K. Andersen (2005), The recurrence time of Dansgaard-Oeschger events and limits on the possible periodic component, *J. Clim.*, *18*(14), 2594–2603, doi:10.1175/jcli3437.1.

Ditlevsen, P. D., K. K. Andersen, and A. Svensson (2007), The DO-climate events are probably noise induced: Statistical investigation of the claimed 1470 years cycle, *Clim. Past*, *3*(1), 129–134.

Dokken, T. M., and E. Jansen (1999), Rapid changes in the mechanism of ocean convection during the last glacial period, *Nature*, *401*(6752), 458–461.

Dokken, T. M., K. H. Nisancioglu, C. Li, D. S. Battisti, and C. Kissel (2013), Dansgaard-Oeschger cycles: Interactions between ocean and sea ice intrinsic to the Nordic seas, *Paleoceanography*, *28*, 491–502, doi:10.1002/palo.20042.
Durack, P. J., and S. E. Wijffels (2010), Fifty-year trends in global ocean salinities and their relationship to broad-scale warming, *J. Clim.*, *23*(16), 4342–4362, doi:10.1175/2010JCLI3377.1.
Eby, M., K. Zickfeld, A. Montenegro, D. Archer, K. Meissner, and A. Weaver (2009), Lifetime of anthropogenic climate change: Millennial time scales of potential $CO_2$ and surface temperature perturbations, *J. Clim.*, *22*(10), 2501–2511, doi:10.1175/2008JCLI2554.1.
EPICA Community Members (2006), One-to-one coupling of glacial climate variability in Greenland and Antarctica, *Nature*, *444*(7116), 195–198, doi:10.1038/nature05301.
Ferrari, R. (2014), Oceanography: What goes down must come up, *Nature*, *513*, 179–180.
Fieg, K., and R. Gerdes (2001), Sensitivity of the thermohaline circulation to modern and glacial surface boundary conditions, *J. Geophys. Res.*, *106*(C4), 6853–6867.
Fyfe, J. C., and O. A. Saenko (2006), Simulated changes in the extratropical Southern Hemisphere winds and currents, *Geophys. Res. Lett.*, *33*, L06701, doi:10.1029/2005GL025332.
Ganopolski, A., and S. Rahmstorf (2001), Rapid changes of glacial climate simulated in a coupled climate model, *Nature*, *409*(6817), 153–158.
Gildor, H., and E. Tziperman (2003), Sea-ice switches and abrupt climate change, *Philos. Trans. R. Soc. A*, *361*(1810), 1935–1944, doi:10.1098/rsta.2003.1244.
Grant, K. M., E. J. Rohling, M. Bar-Matthews, A. Ayalon, M. Medina-Elizalde, C. B. Ramsey, C. Satow, and A. P. Roberts (2012), Rapid coupling between ice volume and polar temperature over the past 150,000 years, *Nature*, *491*, 744–747.
Grootes, P. M., and M. Stuiver (1997), Oxygen 18/16 variability in Greenland snow and ice with $10^{-3}$ to $10^{5}$-year time resolution, *J. Geophys. Res.*, *102*(C12), 26,455–26,470, doi:10.1029/97JC00880.
Guillevic, M., et al. (2013), Spatial gradients of temperature, accumulation and $\delta^{18}$O-ice in Greenland over a series of Dansgaard-Oeschger events, *Clim. Past*, *9*(3), 1029–1051, doi:10.5194/cp-9-1029-2013.
Gutjahr, M., B. A. A. Hoogakker, M. Frank, and I. N. McCave (2010), Changes in north atlantic deep water strength and bottom water masses during marine isotope stage 3 (45–35 ka BP), *Quat. Sci. Rev.*, *29*(19–20), 2451–2461, doi:10.1016/j.quascirev.2010.02.024.
Hallberg, R., and A. Gnanadesikan (2006), The role of eddies in determining the structure and response of the wind-driven Southern Hemisphere overturning: Results from the Modeling Eddies In The Southern Ocean (MESO) project, *J. Phys. Oceanogr.*, *36*(12), 2232–2252, doi:10.1175/jpo2980.1.
Hemming, S. R. (2004), Heinrich events: Massive late Pleistocene detritus layers of the North Atlantic and their global climate imprint, *Rev. Geophys.*, *42*, RG1005, doi:10.1029/2003RG000128.
Hughes, T. M., and A. J. Weaver (1994), Multiple equilibria of an asymmetric two-basin ocean model, *J. Phys. Oceanogr.*, *24*(3), 619–637.
Intergovernmental Panel on Climate Change (IPCC) (2013), *Climate Change 2013: The Physical Science Basis. Contribution of Working Group I to the Fifth Assessment Report of the Intergovernmental Panel on Climate Change*,1535 pp., Cambridge Univ. Press, Cambridge, U. K., and New York, doi:10.1017/CBO9781107415324.
Jouzel, J., et al. (1997), Validity of the temperature reconstruction from water isotopes in ice cores, *J. Geophys. Res.*, *102*(C12), 26,471–26,487, doi:10.1029/97JC01283.
Jouzel, J., F. Vimeux, N. Caillon, G. Delaygue, G. Hoffmann, V. Masson-Delmotte, and F. Parrenin (2003), Magnitude of isotope/temperature scaling for interpretation of Central Antarctic ice cores, *J. Geophys. Res.*, *108*(D12), 4361, doi:10.1029/2002JD002677.
Kageyama, M., A. Paul, D. M. Roche, and C. J. Van Meerbeeck (2010), Modelling glacial climatic millennial-scale variability related to changes in the Atlantic meridional overturning circulation: A review, *Quat. Sci. Rev.*, *29*(21–22), 2931–2956.
Kalnay, E., et al. (1996), The NCEP/NCAR 40-year reanalysis project, *Bull. Am. Meteorol. Soc.*, *77*(3), 437–471, doi:10.1175/1520-0477(1996)077<0437:TNYRP>2.0.CO;2.
Keigwin, L. D., and E. A. Boyle (1999), Surface and deep ocean variability in the Northern Sargasso sea during marine isotope stage 3, *Paleoceanography*, *14*(2), 164–170, doi:10.1029/1998PA900026.
Knorr, G., and G. Lohmann (2003), Southern Ocean origin for the resumption of Atlantic thermohaline circulation during deglaciation, *Nature*, *424*(6948), 532–536, doi:10.1038/nature01855.
Kohfeld, K. E., R. M. Graham, A. M. de Boer, L. C. Sime, E. W. Wolff, C. Le Quéré, and L. Bopp (2013), Southern Hemisphere westerly wind changes during the last glacial maximum: Paleo-data synthesis, *Quat. Sci. Rev.*, *68*, 76–95, doi:10.1016/j.quascirev.2013.01.017.
Kuhlbrodt, T., A. Griesel, M. Montoya, A. Levermann, M. Hofmann, and S. Rahmstorf (2007), On the driving processes of the Atlantic meridional overturning circulation, *Rev. Geophys.*, *45*, RG2001, doi:10.1029/2004RG000166.
Kuhlbrodt, T., S. Rahmstorf, K. Zickfeld, F. B. Vikebø, S. Sundby, M. Hofmann, P. M. Link, A. Bondeau, W. Cramer, and C. Jaeger (2009), An integrated assessment of changes in the thermohaline circulation, *Clim. Change*, *96*(4), 489–537.
Kushner, P. J., I. M. Held, and T. L. Delworth (2001), Southern Hemisphere atmospheric circulation response to global warming, *J. Clim.*, *14*(10), 2238–2249.
Lee, S.-Y., J. C. Chiang, K. Matsumoto, and K. S. Tokos (2011), Southern Ocean wind response to North Atlantic cooling and the rise in atmospheric $CO_2$: Modeling perspective and paleoceanographic implications, *Paleoceanography*, *26*, PA1214, doi:10.1029/2010PA002004.
Lehman, S. J. (1993), Ice sheets, wayward winds and sea change, *Nature*, *365*(6442), 108–110, doi:10.1038/365108a0.
Li, C., D. S. Battisti, D. P. Schrag, and E. Tziperman (2005), Abrupt climate shifts in Greenland due to displacements of the sea ice edge, *Geophys. Res. Lett.*, *32*, L19702, doi:10.1029/2005GL023492.
Lopes Dos Santos, R. A., D. Wilkins, P. D. Deckker, and S. Schouten (2012), Late Quaternary productivity changes from offshore southeastern Australia: A biomarker approach, *Palaeogeogr. Palaeoclimatol. Palaeoecol.*, *363*, 48–56, doi:10.1016/j.palaeo.2012.08.013.
Manabe, S., and R. J. Stouffer (1995), Simulation of abrupt climate change induced by freshwater input to the North Atlantic Ocean, *Nature*, *378*(6553), 165–167.
Marino, G., R. Zahn, M. Ziegler, C. Purcell, G. Knorr, I. R. Hall, P. Ziveri, and H. Elderfield (2013), Agulhas salt-leakage oscillations during abrupt climate changes of the Late Pleistocene, *Paleoceanography*, *28*, 599–606, doi:10.1002/palo.20038.
Marshall, J., and K. Speer (2012), Closure of the meridional overturning circulation through Southern Ocean upwelling, *Nat. Geosci.*, *5*(3), 171–180, doi:10.1038/ngeo1391.
Martrat, B., J. O. Grimalt, N. J. Shackleton, L. de Abreu, M. A. Hutterli, and T. F. Stocker (2007), Four climate cycles of recurring deep and surface water destabilizations on the Iberian margin, *Science*, *317*(5837), 502–507, doi:10.1126/science.1139994.
McManus, J. F., D. W. Oppo, and J. L. Cullen (1999), A 0.5-million-year record of millennial-scale climate variability in the North Atlantic, *Science*, *283*(5404), 971–975, doi:10.1126/science.283.5404.971.
McManus, J. F., R. Francois, J. M. Gherardi, L. D. Keigwin, and S. Brown-Leger (2004), Collapse and rapid resumption of Atlantic meridional circulation linked to deglacial climate changes, *Nature*, *428*(6985), 834–837, doi:10.1038/nature02494.

Mix, A. C., W. F. Ruddiman, and A. McIntyre (1986), Late Quaternary paleoceanography of the tropical Atlantic, 1: Spatial variability of annual mean sea-surface temperatures, 0–20,000 years B.P., *Paleoceanography*, *1*(1), 43–66, doi:10.1029/PA001i001p00043.
NGRIP Community Members (2004), High-resolution record of Northern Hemisphere climate extending into the last interglacial period, *Nature*, *431*(7005), 147–151, doi:10.1038/nature02805.
Obrochta, S. P., Y. Yokoyama, J. Morén, and T. J. Crowley (2014), Conversion of GISP2-based sediment core age models to the GICC05 extended chronology, *Quat. Geochronol.*, *20*, 1–7.
Oppo, D. W., and S. J. Lehman (1995), Suborbital timescale variability of North Atlantic deep water during the past 200,000 years, *Paleoceanography*, *10*(5), 901–910, doi:10.1029/95PA02089.
Parrenin, F., V. Masson-Delmotte, P. Köhler, D. Raynaud, D. Paillard, J. Schwander, C. Barbante, A. Landais, A. Wegner, and J. Jouzel (2013), Synchronous change of atmospheric $CO_2$ and Antarctic temperature during the last deglacial warming, *Science*, *339*(6123), 1060–1063, doi:10.1126/science.1226368.
Peeters, F. J. C., R. Acheson, G.-J. A. Brummer, W. P. M. de Ruijter, R. R. Schneider, G. M. Ganssen, E. Ufkes, and D. Kroon (2004), Vigorous exchange between the Indian and Atlantic oceans at the end of the past five glacial periods, *Nature*, *430*(7000), 661–665.
Peltier, W. R. (1994), Ice age paleotopography, *Science*, *265*, 195–195.
Petersen, S. V., D. P. Schrag, and P. U. Clark (2013), A new mechanism for Dansgaard-Oeschger cycles, *Paleoceanography*, *28*, 24–30, doi:10.1029/2012PA002364.
Piotrowski, A. M., S. L. Goldstein, S. R. Hemming, R. G. Fairbanks, and D. R. Zylberberg (2008), Oscillating glacial northern and southern deep water formation from combined neodymium and carbon isotopes, *Earth Planet. Sci. Lett.*, *272*(1–2), 394–405, doi:10.1016/j.epsl.2008.05.011.
Purkey, S. G., and G. C. Johnson (2012), Global contraction of Antarctic bottom water between the 1980s and 2000s*, *J. Clim.*, *25*(17), 5830–5844, doi:10.1175/jcli-d-11-00612.1.
Rahmstorf, S. (1996), On the freshwater forcing and transport of the Atlantic thermohaline circulation, *Clim. Dyn.*, *12*(12), 799–811.
Rahmstorf, S. (2002), Ocean circulation and climate during the past 120,000 years, *Nature*, *419*(6903), 207–214, doi:10.1038/nature01090.
Rahmstorf, S., and M. H. England (1997), Influence of Southern Hemisphere winds on North Atlantic deep water flow, *J. Phys. Oceanogr.*, *27*(9), 2040–2054.
Rasmussen, S. O., et al. (2006), A new Greenland ice core chronology for the last glacial termination, *J. Geophys. Res.*, *111*, D06102, doi:10.1029/2005JD006079.
Rasmussen, S. O., et al. (2013), A first chronology for the north Greenland Eemian ice drilling (NEEM) ice core, *Clim. Past*, *9*(6), 2713–2730, doi:10.5194/cp-9-2713-2013.
Rohling, E. J., K. Grant, M. Bolshaw, A. P. Roberts, M. Siddall, Ch. Hemleben, and M. Kucera (2009), Antarctic temperature and global sea level closely coupled over the past five glacial cycles, *Nat. Geosci.*, *2*(7), 500–504, doi:10.1038/ngeo557.
Rojas, M., P. Moreno, M. Kageyama, M. Crucifix, C. Hewitt, A. Abe-Ouchi, R. Ohgaito, E. C. Brady, and P. Hope (2009), The southern westerlies during the last glacial maximum in PMIP2 simulations, *Clim. Dyn.*, *32*(4), 525–548.
Saenko, O. A., A. J. Weaver, and A. Schmittner (2003), Atlantic deep circulation controlled by freshening in the Southern Ocean, *Geophys. Res. Lett.*, *30*(14), 1754, doi:10.1029/2003GL017681.
Schmittner, A., T. A. M. Silva, K. Fraedrich, E. Kirk, and F. Lunkeit (2011), Effects of Mountains and Ice Sheets on Global Ocean Circulation, *J. Clim.*, *24*(11), 2814–2829, doi:10.1175/2010JCLI3982.1.
Schulz, M. (2002), On the 1470-year pacing of Dansgaard-Oeschger warm events, *Paleoceanography*, *17*(2), 1014, doi:10.1029/2000PA000571.
Schulz, M., W. H. Berger, M. Sarnthein, and P. M. Grootes (1999), Amplitude variations of 1470-year climate oscillations during the last 100,000 years linked to fluctuations of continental ice mass, *Geophys. Res. Lett.*, *26*(22), 3385–3388.
Seager, R., and D. S. Battisti (2007), Challenges to our understanding of the general circulation: Abrupt climate change, in *The Global Circulation of the Atmosphere: Phenomena, Theory, Challenges*, edited by T. Schneider and A. H. Sobel, pp. 331–371, Princeton Univ. Press, Princeton, N. J.
Seidov, D., E. Barron, and B. J. Haupt (2001), Meltwater and the global ocean conveyor: Northern versus southern connections, *Global Planet. Change*, *30*(3), 257–270.
Sijp, W. P., and M. H. England (2008), The effect of a northward shift in the Southern Hemisphere westerlies on the global ocean, *Prog. Oceanogr.*, *79*(1), 1–19, doi:10.1016/j.pocean.2008.07.002.
Sijp, W. P., and M. H. England (2009), Southern Hemisphere westerly wind control over the ocean's thermohaline circulation, *J. Clim.*, *22*(5), 1277–1286.
Sikes, E. L., W. R. Howard, C. R. Samson, T. S. Mahan, L. G. Robertson, and J. K. Volkman (2009), Southern Ocean seasonal temperature and subtropical front movement on the South Tasman rise in the Late Quaternary, *Paleoceanography*, *24*, PA2201, doi:10.1029/2008PA001659.
Sima, A., A. Paul, and M. Schulz (2004), The younger dryas—An intrinsic feature of Late Pleistocene climate change at millennial timescales, *Earth Planet. Sci. Lett.*, *222*(3), 741–750.
Sime, L. C., K. E. Kohfeld, C. Le Quéré, E. W. Wolff, A. M. de Boer, R. M. Graham, and L. Bopp (2013), Southern Hemisphere westerly wind changes during the last glacial maximum: Model-data comparison, *Quat. Sci. Rev.*, *64*, 104–120.
Srokosz, M. A., and H. L. Bryden (2015), Observing the Atlantic meridional overturning circulation yields a decade of inevitable surprises, *Science*, *348*(6241), 1,255,575, doi:10.1126/science.1255575.
Stocker, T. F., and S. J. Johnsen (2003), A minimum thermodynamic model for the bipolar seesaw, *Paleoceanography*, *18*(4), 1087, doi:10.1029/2003PA000920.
Talley, L. D. (2013), Closure of the global overturning circulation through the Indian, Pacific, and Southern Oceans: Schematics and transports, *Oceanography*, *26*, 80–97.
Thompson, D. W., and S. Solomon (2002), Interpretation of recent Southern Hemisphere climate change, *Science*, *296*(5569), 895–899.
Toggweiler, J. R., and J. Russell (2008), Ocean circulation in a warming climate, *Nature*, *451*(7176), 286–288, doi:10.1038/nature06590.
Toggweiler, J. R., and B. Samuels (1995), Effect of drake passage on the global thermohaline circulation, *Deep Sea Res., Part I*, *42*(4), 477–500, doi:10.1016/0967-0637(95)00012-u.
Toggweiler, J. R., J. L. Russell, and S. R. Carson (2006), Midlatitude westerlies, atmospheric $CO_2$, and climate change during the ice ages, *Paleoceanography*, *21*(2), PA2005, doi:10.1029/2005PA001154.
Ullman, D. J., A. N. LeGrande, A. E. Carlson, F. S. Anslow, and J. M. Licciardi (2014), Assessing the impact of Laurentide ice sheet topography on glacial climate, *Clim. Past*, *10*(2), 487–507, doi:10.5194/cp-10-487-2014.

Vidal, L., L. Labeyrie, E. Cortijo, M. Arnold, J. C. Duplessy, E. Michel, S. Becqué, and T. C. E. van Weering (1997), Evidence for changes in the North Atlantic deep water linked to meltwater surges during the Heinrich events, *Earth Planet. Sci. Lett.*, *146*(1–2), 13–27, doi:10.1016/S0012-821X(96)00192-6.

Völker, C., and P. Köhler (2013), Responses of ocean circulation and carbon cycle to changes in the position of the Southern Hemisphere westerlies at last glacial maximum, *Paleoceanography*, *28*, 726–739, doi:10.1002/2013PA002556.

WAIS Divide Project Members (2015), Precise interpolar phasing of abrupt climate change during the last ice age, *Nature*, *520*(7549), 661–665, doi:10.1038/nature14401.

Wang, Z., and L. A. Mysak (2006), Glacial abrupt climate changes and Dansgaard-Oeschger oscillations in a coupled climate model, *Paleoceanography*, *21*, PA2001, doi:10.1029/2005PA001238.

Weaver, A. J., et al. (2001), The Uvic Earth system climate model: Model description, climatology, and applications to past, present and future climates, *Atmos. Ocean*, *39*(4), 361–428.

Wunsch, C. (2006), Abrupt climate change: An alternative view, *Quat. Res.*, *65*(2), 191–203, doi:10.1016/j.yqres.2005.10.006.

Yin, J. H. (2005), A consistent poleward shift of the storm tracks in simulations of 21st century climate, *Geophys. Res. Lett.*, *32*, L18701, doi:10.1029/2005GL023684.

Yung, Y. L., T. Lee, C.-H. Wang, and Y.-T. Shieh (1996), Dust: A diagnostic of the hydrologic cycle during the last glacial maximum, *Science*, *271*(5251), 962–963, doi:10.1126/science.271.5251.962.

Zahn, R., J. Schönfeld, H. Kudrass, M. Park, H. Erlenkeuser, and P. Grootes (1997), Thermohaline instability in the North Atlantic during meltwater events: Stable isotope and ice-rafted detritus records from core SO75-26KL, Portuguese margin, *Paleoceanography*, *12*(5), 696–710.

Zhang, X., G. Lohmann, G. Knorr, and C. Purcell (2014), Abrupt glacial climate shifts controlled by ice sheet changes, *Nature*, *512*(7514), 290–294, doi:10.1038/nature13592.

Zhu, J., Z. Liu, X. Zhang, I. Eisenman, and W. Liu (2014), Linear weakening of the AMOC in response to receding glacial ice sheets in CCSM3, *Geophys. Res. Lett.*, *41*, 6252–6258, doi:10.1002/2014GL060891.